

A DYNAMICAL MODEL FOR URBAN HEAT ISLANDS

JONG-JIN BAIK

Department of Environmental Science and Engineering, Kwangju Institute of Science and Technology, Kwangju 506-303, Korea

HYE-YEONG CHUN

Department of Astronomy and Atmospheric Sciences, Yonsei University, Seoul 120-749, Korea

(Received in final form 7 February, 1997)

Abstract. Effects of nonlinearity on the airflow past an urban heat island and precipitation change downwind, are investigated analytically in the context of the weakly nonlinear response of a stably stratified uniform flow to specified heating. The heating structure is assumed to be bell-shaped in the horizontal and exponentially decreasing with height. The forcing to the first-order equation exhibits cooling in the concentrated low-level heating region. The linear solution component shows upward motion downstream as suggested by many previous studies. The weakly nonlinear solution component shows downward or upward motion downstream depending on the heating depth. It is proposed that when the heating depth is large, but still within a valid range of the perturbation expansion, the linear and weakly nonlinear effects constructively work together to produce enhanced upward motion on the downstream side, not far from the heating centre. This explains to a greater extent the precipitation enhancement downstream of the heat island than is possible from the linear effect alone. It is also proposed that when the heating depth is small, the linear and weakly nonlinear effects destructively work together to reduce upward motion on the downstream side, not far from the heating centre. This explains to a greater extent the lack of precipitation enhancement downstream than is possible from the linear effect alone.

Key words: Urban heat island, Stably stratified flow, Diabatic forcing, Weakly nonlinear response, Internal gravity wave.

1. Introduction

An interesting effect of the urban heat-island phenomenon is a tendency for precipitation enhancement on the downstream side of the heat island. Changnon et al. (1991) found an increase in precipitation downwind of the St. Louis area by 17% during autumn and 4% during spring. Airflow characteristics past the urban heat island can be examined theoretically in the context of the response of a stably stratified flow to specified surface or finite-depth heating which represents temperature excess in the heat island region. Linear studies along this research line (Olfe and Lee, 1971; Lin and Smith, 1986; Baik, 1992) indicate a negative phase relationship between the heating and the induced vertical motion in the vicinity of the heating centre and upward motion downstream. This upward motion is suggested to be partly responsible for precipitation enhancement downstream of the heat island (Lin and Smith, 1986).

Since the heating associated with the urban heat island is typically small compared with, for example, the heating due to deep cumulus convection, the flow regime might be approximately linear. However, the flow can deviate from a linear

regime as the heating amplitude, horizontal length scale of the heating, stability or basic-state wind vary in a certain way (Baik and Chun, 1996). A numerical model enables us to examine nonlinear effects on the airflow past the heat island (Baik, 1992). A nonlinear theoretical approach, even if in a very simple flow system, can provide a clear dynamical insight of how nonlinearity plays a role in such a flow system. However, the fully nonlinear problem appears to be extremely difficult to solve.

In this study, to investigate the effects of nonlinearity on the airflow past the urban heat island and precipitation downwind, the previous linear theoretical studies are extended by including weak nonlinearity. The present weakly nonlinear approach is the same as that of Chun and Baik (1994) except that the vertical heating profile is exponentially decreasing. In terms of an application to the urban heat island, this profile is more appropriate than the uniform heating profile. In Section 2, governing equations and linear and weakly nonlinear solutions are presented. Results are given and discussed in Section 3 and concluding remarks follow in Section 4.

2. Governing Equations and Solutions

Consider a two-dimensional, steady-state, hydrostatic, nonrotating, inviscid, Boussinesq airflow system in a uniform basic-state horizontal wind with diabatic forcing. The nondimensionalized equation set governing perturbations can be expressed by (Baik and Chun, 1996)

$$\frac{\partial u}{\partial x} + \mu \left(u \frac{\partial u}{\partial x} + w \frac{\partial u}{\partial z} \right) = - \frac{\partial \pi}{\partial x}, \quad (1)$$

$$\frac{\partial b}{\partial x} + w + \mu \left(u \frac{\partial b}{\partial x} + w \frac{\partial b}{\partial z} \right) = q, \quad (2)$$

$$\frac{\partial u}{\partial x} + \frac{\partial w}{\partial z} = 0, \quad (3)$$

$$\frac{\partial \pi}{\partial z} = b. \quad (4)$$

Here, x is the horizontal coordinate, z the vertical coordinate, u the perturbation wind velocity in the x direction, w the perturbation wind velocity in the z direction, π the perturbation kinematic pressure, b the perturbation buoyancy, and q the diabatic forcing (in this study, all the variables are nondimensional ones unless otherwise mentioned). The parameter μ in (1) and (2) is the nonlinearity factor of the thermally-induced finite-amplitude waves given by $\mu = g q_a L / (c_p T_0 N U^2)$, where g is the gravitational acceleration, q_a the dimensional amplitude of the diabatic forcing, L the dimensional horizontal length scale of the diabatic forcing, c_p the specific heat of air at constant pressure, T_0 the dimensional constant reference

temperature, N the Brunt–Vaisala frequency of the basic flow, and U the dimensional basic-state horizontal wind ($U > 0$ in this study). The nonlinearity factor μ represents a scale ratio of the perturbation horizontal wind to the basic-state wind (Lin and Chun, 1991). In this study, the diabatic forcing is assumed to be bell-shaped in the horizontal and exponentially decreasing with height,

$$q(x, z) = \left(\frac{a_1^2}{x^2 + a_1^2} - \frac{a_1 a_2}{x^2 + a_2^2} \right) e^{-z/h}. \quad (5)$$

Here, a_1 (half-width of the bell-shaped function) and a_2 are constants with $a_1 < a_2$ and h is the e -folding heating depth. Note that, in dimensional terms, $a_1 \approx 0.5 L$. The widespread cooling term is included to avoid the net heating problem in a steady-state, inviscid flow system (Smith and Lin, 1982).

With an introduction of the streamfunction φ that satisfies $\partial\varphi/\partial x = -w$ and $\partial\varphi/\partial z = u$, Equations (1)–(4) can be combined to yield the following two equations in φ and b ,

$$\frac{\partial^3 \varphi}{\partial x \partial z^2} + \frac{\partial b}{\partial x} - \mu J \left(\varphi, \frac{\partial^2 \varphi}{\partial z^2} \right) = 0, \quad (6)$$

$$\frac{\partial b}{\partial x} - \frac{\partial \varphi}{\partial x} - \mu J(\varphi, b) = q, \quad (7)$$

where J represents the Jacobian defined by $J(A, B) = (\partial A/\partial x)(\partial B/\partial z) - (\partial A/\partial z)(\partial B/\partial x)$. To analytically obtain linear (zeroth-order) solutions in physical space and weakly nonlinear (first-order) solutions in wavenumber space, we follow the procedure described in Chun and Baik (1994). To apply the perturbation method to the above two equations, the streamfunction and buoyancy are expanded in small values of the nonlinearity factor μ ; $\varphi = \varphi_0 + \mu\varphi_1 + \mu^2\varphi_2 + \dots$ and $b = b_0 + \mu b_1 + \mu^2 b_2 + \dots$. The diabatic forcing is assumed to have only a zeroth order term, that is, $q = q_0$. Substituting these expansions in φ , b , and q into Equations (6) and (7), and using the relationships $\partial\varphi_0/\partial x = -w_0$ and $\partial\varphi_1/\partial x = -w_1$, gives equations of the lowest two powers in the vertical velocity

$$\frac{\partial^2 w_0}{\partial z^2} + w_0 = q_0, \quad (8)$$

$$\frac{\partial^2 w_1}{\partial z^2} + w_1 = F(x, z), \quad (9)$$

where

$$F(x, z) = -J \left(\varphi_0, \frac{\partial^2 \varphi_0}{\partial z^2} - b_0 \right). \quad (10)$$

Taking the Fourier transform of Equation (8) gives

$$\frac{\partial^2 \tilde{w}_0}{\partial z^2} + \tilde{w}_0 = \tilde{q}_0. \quad (11)$$

The general solution to Equation (11) is

$$\tilde{w}_0(k, z) = A_0(k)e^{iz} + B_0(k)e^{-iz} + \alpha \tilde{f}(k)e^{-z/h}, \quad (12)$$

where $\alpha = 1/(1 + 1/h^2)$ and $\tilde{f}(k) = a_1(e^{-a_1 k} - e^{-a_2 k})$, and k is the horizontal wavenumber. To determine the two unknown coefficients $A_0(k)$ and $B_0(k)$, we impose the flat bottom boundary condition ($\tilde{w}_0 = 0$ at $z = 0$) and the upper radiation condition (Booker and Bretherton, 1967), which requires $B_0(k) = 0$. Then, Equation (12) becomes

$$\tilde{w}_0(k, z) = \alpha \tilde{f}(k)(e^{-z/h} - e^{iz}). \quad (13)$$

After taking the inverse Fourier transform of Equation (13), the zeroth-order solution for the vertical velocity in physical space is obtained, viz.

$$w_0(x, z) = \alpha[X_1(e^{-z/h} - \cos z) + X_2 \sin z], \quad (14)$$

where $X_1 = a_1^2/(x^2 + a_1^2) - a_1 a_2/(x^2 + a_2^2)$ and $X_2 = a_1 x/(x^2 + a_1^2) - a_1 x/(x^2 + a_2^2)$. It can be easily shown that the zeroth-order solutions for the streamfunction, horizontal velocity, and buoyancy are given, respectively, by

$$\varphi_0(x, z) = -\alpha[X_3(e^{-z/h} - \cos z) + X_4 \sin z], \quad (15)$$

$$u_0(x, z) = \frac{\alpha}{h}[X_3(e^{-z/h} - h \sin z) - h X_4 \cos z], \quad (16)$$

$$b_0(x, z) = -\alpha[X_3(e^{-z/h} - \cos z) + X_4 \sin z] + X_3 e^{-z/h}, \quad (17)$$

where $X_3 = a_1[\tan^{-1}(x/a_1) - \tan^{-1}(x/a_2)]$ and $X_4 = (a_1/2) \ln[(x^2 + a_1^2)/(x^2 + a_2^2)]$.

The forcing term (10) in the first-order Equation (9) is determined by the zeroth-order perturbation and can be written as

$$F(x, z) = \frac{2\alpha}{h}e^{-z/h}[X_1 X_3(h \sin z - \cos z) + X_2 X_3 \sin z + h X_1 X_4 \cos z]. \quad (18)$$

Taking the Fourier transform of Equation (9) gives

$$\frac{\partial^2 \tilde{w}_1}{\partial z^2} + \tilde{w}_1 = \tilde{F}. \quad (19)$$

The general solution to Equation (19) can be shown to be

$$\tilde{w}_1(k, z) = A_1(k)e^{iz} + B_1(k)e^{-iz} - \frac{i}{2}[\tilde{S}(k, z)e^{iz} - \tilde{T}(k, z)e^{-iz}]. \quad (20)$$

Here, the functions $S(x, z)$ and $T(x, z)$ are expressed by

$$\begin{aligned} S(x, z) = & -\gamma e^{-z/h}[(X_1 X_3 - h X_1 X_4)(2h\beta \sin 2z - \beta \cos 2z - 4h^2) \\ & + \beta(h X_1 X_3 + X_2 X_3)(\sin 2z + 2h \cos 2z)] \\ & + i\gamma e^{-z/h}[(h X_1 X_3 + X_2 X_3)(2h\beta \sin 2z - \beta \cos 2z + 4h^2) \\ & - \beta(X_1 X_3 - h X_1 X_4)(\sin 2z + 2h \cos 2z)], \end{aligned} \quad (21)$$

$$\begin{aligned} T(x, z) = & -\gamma e^{-z/h}[(X_1 X_3 - h X_1 X_4)(2h\beta \sin 2z - \beta \cos 2z - 4h^2) \\ & + \beta(h X_1 X_3 + X_2 X_3)(\sin 2z + 2h \cos 2z)] \\ & - i\gamma e^{-z/h}[(h X_1 X_3 + X_2 X_3)(2h\beta \sin 2z - \beta \cos 2z + 4h^2) \\ & - \beta(X_1 X_3 - h X_1 X_4)(\sin 2z + 2h \cos 2z)], \end{aligned} \quad (22)$$

where $\beta = 1/[1 + 1/(4h^2)]$ and $\gamma = \alpha/(4h^2)$. As was done in the procedure of finding the zeroth-order solution, the two unknown coefficients $A_1(k)$ and $B_1(k)$ in Equation (20) are determined by imposing the flat bottom boundary condition and the upper radiation condition. Then, the first-order solution for the vertical velocity in wavenumber space becomes

$$\tilde{w}_1(k, z) = \frac{i}{2}\{[\tilde{S}(k, 0) - \tilde{T}(k, 0)]e^{iz} - \tilde{S}(k, z)e^{iz} + \tilde{T}(k, z)e^{-iz}\}. \quad (23)$$

The first-order solutions for the streamfunction, horizontal velocity, and buoyancy can be obtained, respectively, by

$$\tilde{\varphi}_1(k, z) = \frac{i}{k}\tilde{w}_1(k, z), \quad (24)$$

$$\tilde{u}_1(k, z) = \frac{i}{k} \frac{\partial \tilde{w}_1(k, z)}{\partial z}, \quad (25)$$

$$\tilde{b}_1(k, z) = \tilde{\varphi}_1(k, z) - \frac{i}{2k}\tilde{F}(k, z). \quad (26)$$

To get the first-order solutions in physical space, a fast Fourier transform (FFT) technique is used. The computational domain size in the x direction is 51.1 with the number of the horizontal waves of 512, and the computational domain size in the z direction is 10 with a vertical grid resolution of 0.05. The length scales a_1 and a_2 are set to $a_1 = 1$ and $a_2 = 5a_1$.

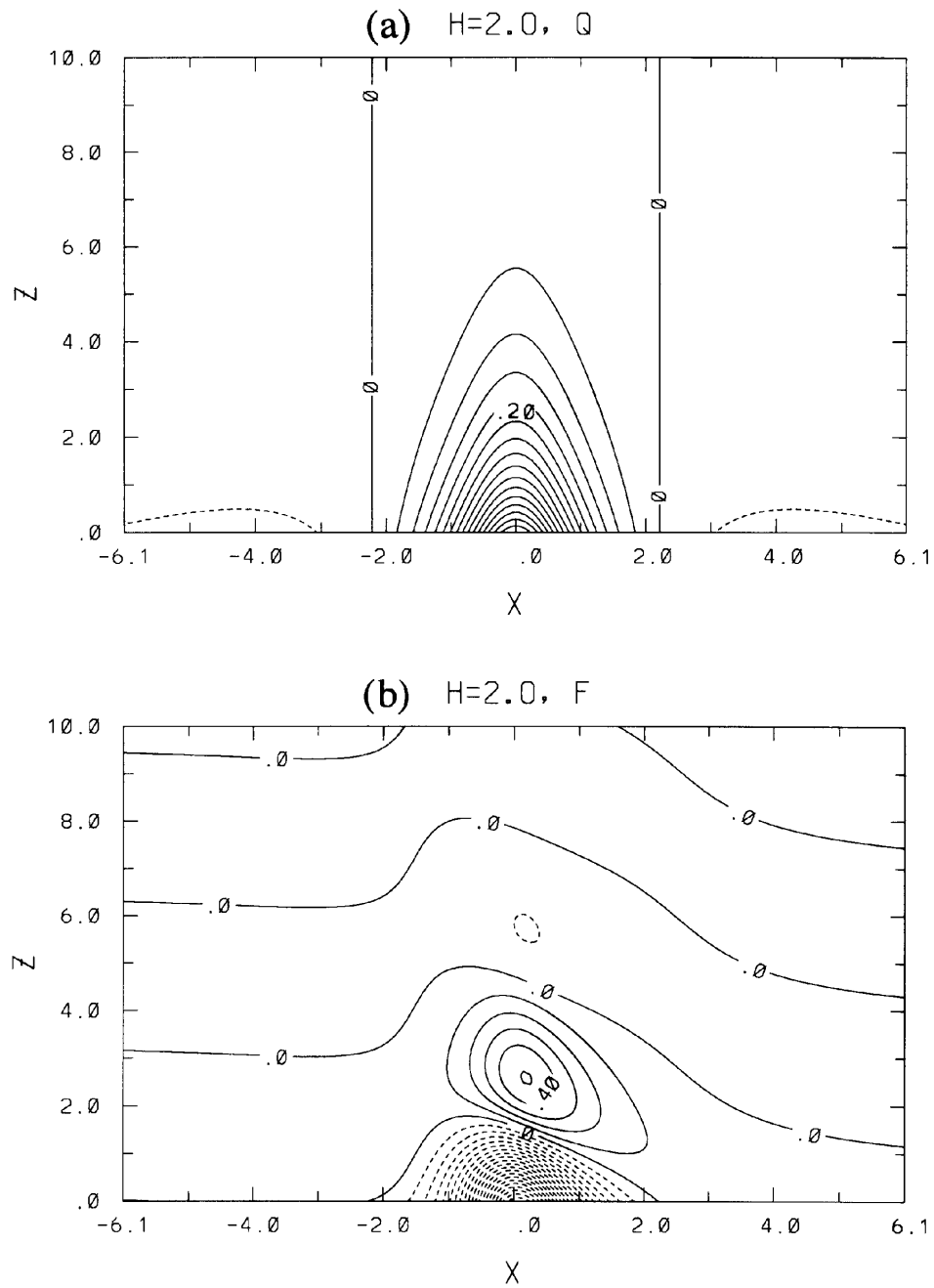


Figure 1. The fields of (a) the specified heating q and (b) the forcing function F to the first-order equation for the case of $h = 2$. Contour intervals in (a) and (b) are 0.05 and 0.1 respectively.

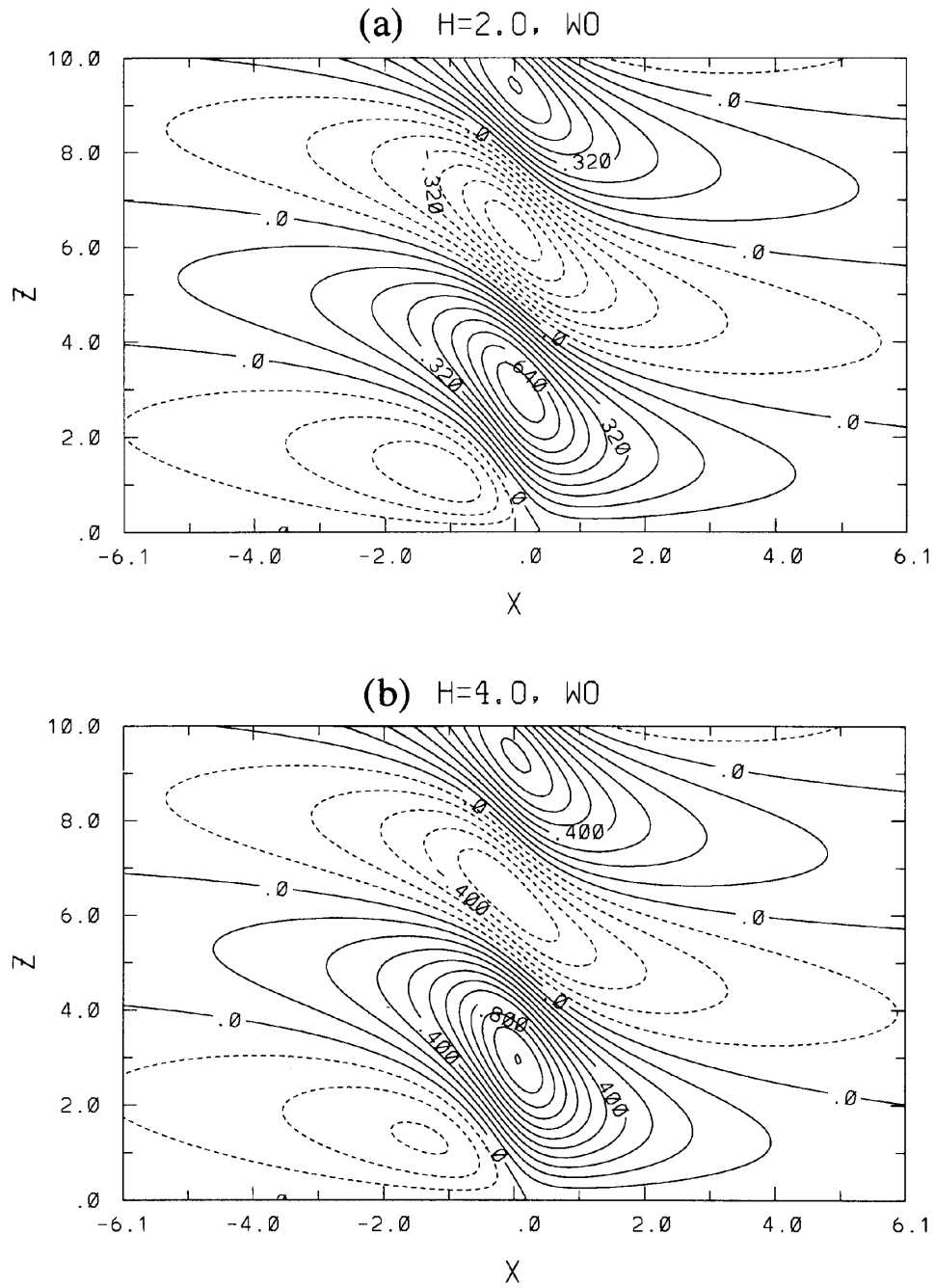


Figure 2. The zeroth-order perturbation vertical velocity fields for the cases of (a) $h = 2$ and (b) $h = 4$. Contour intervals in (a) and (b) are 0.08 and 0.1 respectively.

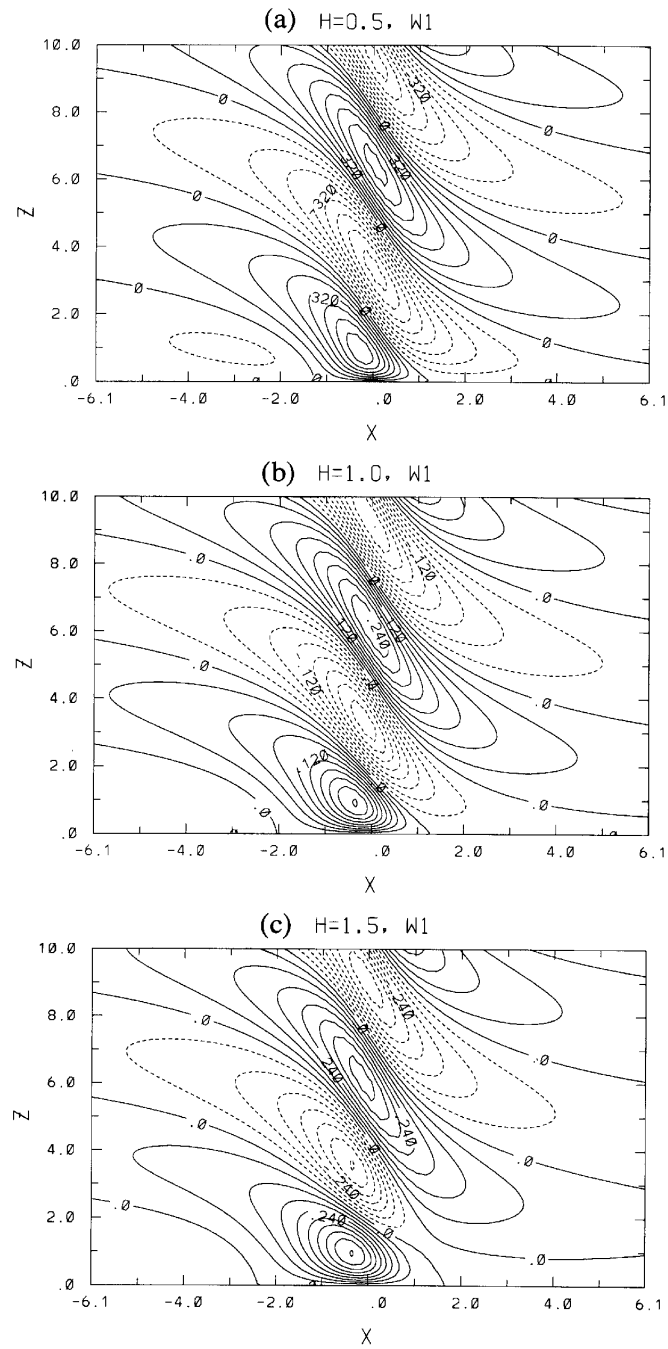
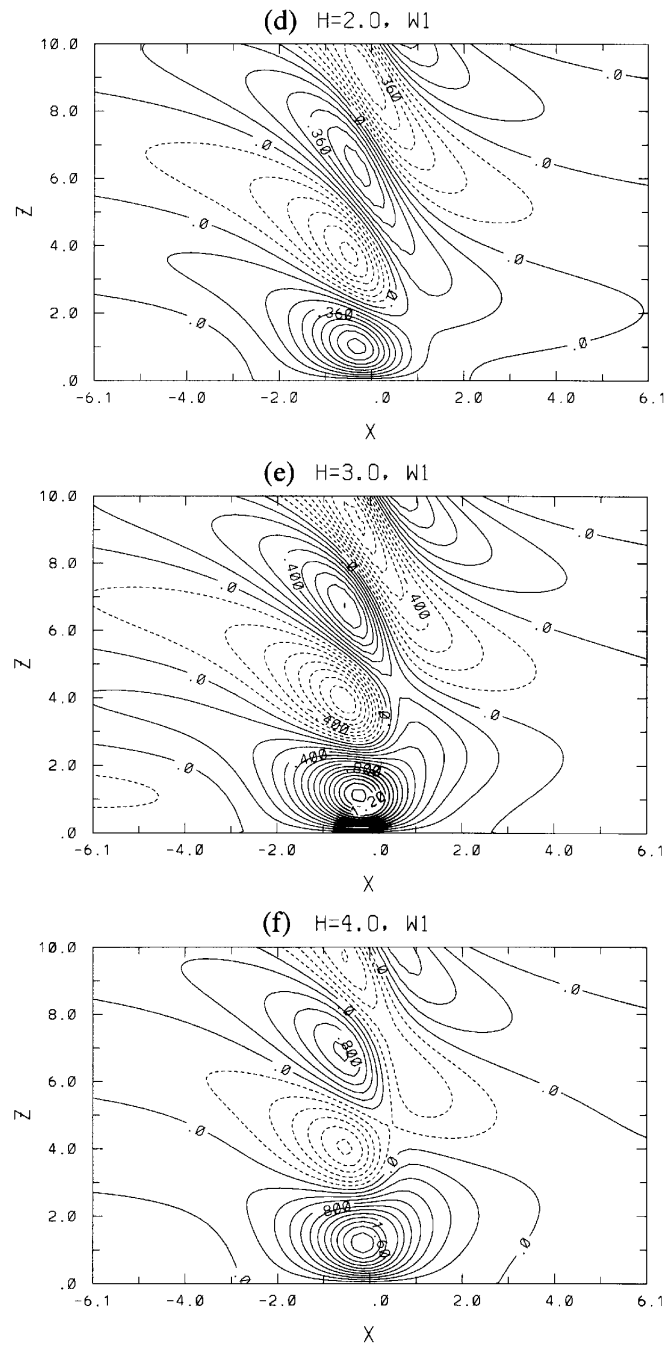


Figure 3. The first-order perturbation vertical velocity fields for the cases of (a) $h = 0.5$, (b) $h = 1$, (c) $h = 1.5$, (d) $h = 2$, (e) $h = 3$, and (f) $h = 4$. The values in the field (a) are scaled by 10000 and the contour interval is 80. Contour intervals in (b)–(f) are 0.03, 0.06, 0.09, 0.1, and 0.2 respectively.

*Figure 3. Continued.*

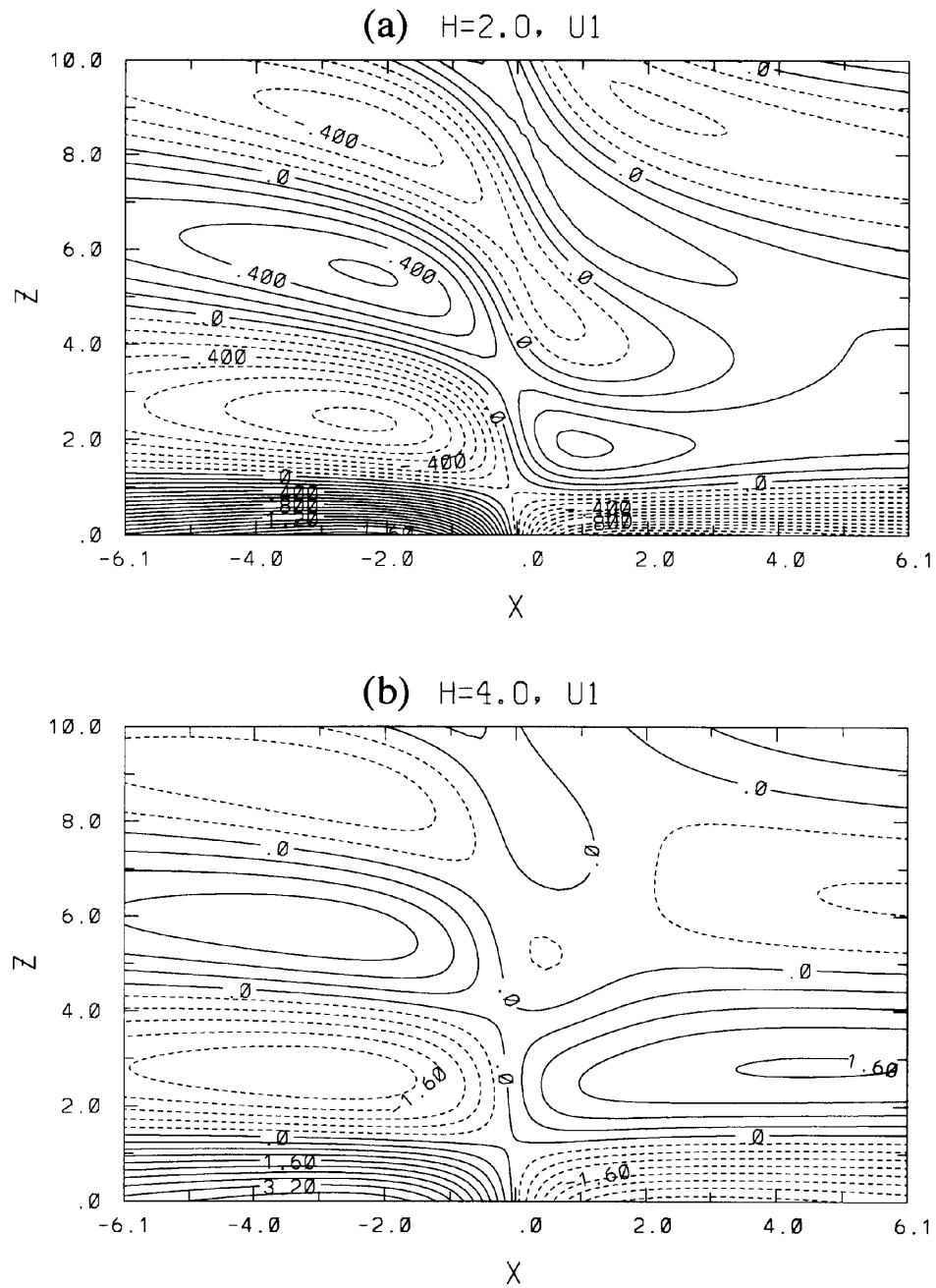


Figure 4. The first-order perturbation horizontal velocity fields for the cases of (a) $h = 2$ and (b) $h = 4$. Contour intervals in (a) and (b) are 0.1 and 0.4 respectively.

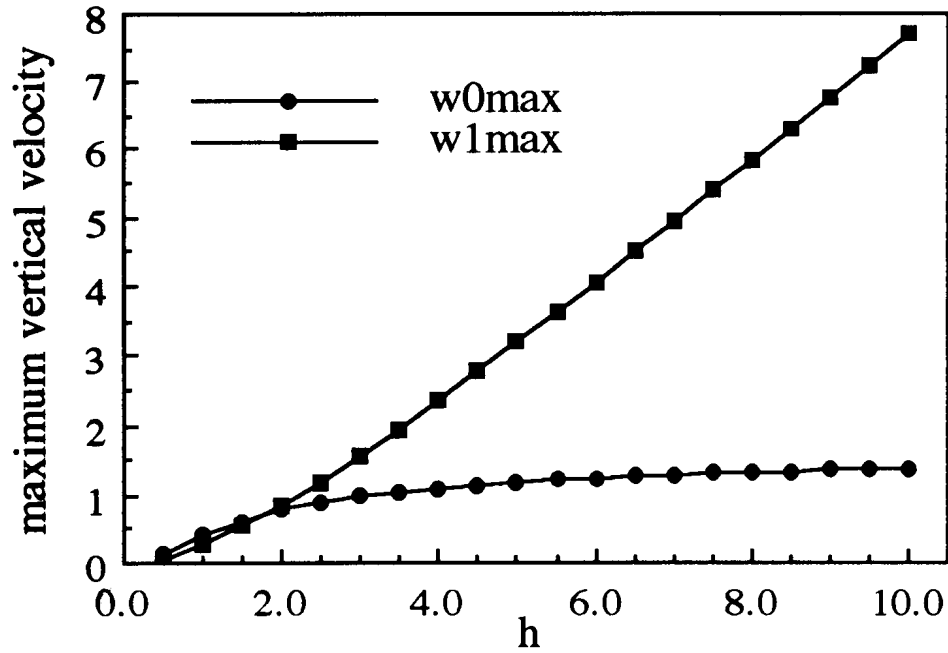


Figure 5. The domain maximum zeroth-order and first-order perturbation vertical velocities as a function of h .

3. Results and Discussion

Figure 1 shows the fields of the specified heating q (Equation (5)) and the forcing function F (Equation (18)) to the first-order equation for an e -folding heating depth h of 2. (Note that the nondimensional $h = Nh_a/U$ (an inverse Froude number), with h_a the dimensional e -folding heating depth; taking dimensional values of $N = 0.01 \text{ s}^{-1}$, $h_a = 700 \text{ m}$, and $U = 3.5 \text{ m s}^{-1}$ for an urban heat island gives $h = 2$.) In the q field, the heating exists in the region of $-5^{1/2} < x < 5^{1/2}$ and the cooling exists outside of this region. The forcing function F exhibits cooling in the concentrated low-level heating region, and above the cooling region alternating heating and cooling are observed with the magnitude of the forcing maximum in each region decreasing with height. Since the forced cooling and heating are calculated using the zeroth-order solutions that are tilted upstream, they are also tilted upstream. At $x = 0$, $F(0, z) = [2\alpha a_1 e^{-z/h} (1 - a_1/a_2) \ln(a_1/a_2)] \cos z$. Thus, $F(0, z)$ becomes zero at heights of $z = (n + 1/2)\pi$, $n = 0, 1, 2, 3, \dots$. The net horizontal heating at any height is zero in the specified heating q , while it is not zero in the forcing function F except at heights of

$$z = n\pi - \tan^{-1} \left[h \int_{-\infty}^{\infty} X_1 X_4 dx / \int_{-\infty}^{\infty} X_2 X_3 dx \right]. \quad (27)$$

Since

$$\int_{-\infty}^{\infty} X_1 X_4 \, dx = - \int_{-\infty}^{\infty} X_2 X_3 \, dx,$$

Equation (27) is equivalent to

$$z = n\pi + \tan^{-1} h. \quad (28)$$

The first-order solutions may not be bounded at infinity except for the specific heights given by Equation (28). For the case of $h = 2$, the first height at which the net horizontal heating becomes zero is located at $z = 1.107$.

The zeroth-order perturbation vertical velocity fields for the cases of $h = 2$ and 4 are shown in Figure 2. The vertical velocity fields (w_0) reveal typical features that gravity waves produce in response to the thermal forcing in the presence of the basic-state wind. These include the bands of positive and negative perturbations with upstream phase tilt, implying upward energy propagation, and a vertical wavelength of 2π (in a nondimensional form). The w_0 fields in the lower layer show downward motion on the upstream side of the heating and upward motion on the downstream side, as suggested by previous linear studies (Olfe and Lee, 1971; Smith and Lin, 1982; Lin and Smith, 1986; Baik, 1992).

To examine how the e -folding heating depth affects the weakly nonlinear response, the first-order perturbation vertical velocity fields with different heating depths ($h = 0.5, 1, 1.5, 2, 3$, and 4) are presented in Figure 3. All the first-order vertical velocity fields exhibit upstream phase tilt, implying upward energy propagation, and upward motion in the concentrated low-level forcing region. As in the w_0 fields (Figure 2), the vertical wavelength in all the w_1 fields is 2π , because the vertical wavelength of internal gravity wave in a stably stratified atmosphere is related to the basic-state wind and the basic-state stability (Brunt–Vaisala frequency). As the heating depth increases, this updraft region tends to extend downstream and vertically and the magnitude of the perturbation vertical velocity increases. For small values of the heating depth (say, $h = 0.5$ case), the w_1 field in the lower layer shows downward motion downstream (Figure 3a). On the other hand, for large values of the heating depth (say, $h = 3$ case), the w_1 field in the lower layer shows upward motion to some distance on the downstream side (Figure 3e). For the dimensional values of $q_0 = 0.1 \, \text{J kg}^{-1} \, \text{s}^{-1}$, $T_0 = 15^\circ\text{C}$, and $N = 0.01 \, \text{s}^{-1}$, the nondimensional perturbation vertical velocity ($w = w_0 + \mu w_1$) of 1 corresponds to the dimensional perturbation vertical velocity of $3.4 \, \text{cm s}^{-1}$ (see Baik and Chun, 1996, for the scale factor).

A comparison of Figures 2 and 3 indicates that the tilting slope of upstream phase in the first-order vertical velocity field is larger than that in the zeroth-order vertical velocity field. The tilting slope of the phase of plane wave can be expressed by $z/x = -\lambda_z/\lambda_x = -k/m$ (dimensional variables), where λ_x and λ_z are the horizontal and vertical wavelengths respectively, and m is the vertical wavenumber;

λ_x is proportionally dependent upon the characteristic horizontal forcing scale. Therefore, as the horizontal forcing scale becomes smaller, the upstream phase tilt becomes closer to vertical. The larger tilting slope of the upstream phase in the w_1 field compared to that in the w_0 field is believed to be due to the smaller characteristic horizontal scale in the concentrated forcing region associated with the first-order field (forcing F) than that associated with the zeroth-order field (forcing q).

Figure 4 shows the first-order perturbation horizontal velocity fields for the cases of $h = 2$ and 4, which correspond to Figures 3d and 3f respectively. In the lower layer, the first-order perturbation horizontal velocity is positive on the upstream side and negative on the downstream side, thus producing a strong convergence near the forcing centre. This convergence is responsible for the upward motion near the forcing centre (Figures 3d and 3f). The magnitude of the perturbation horizontal velocity in the $h = 4$ case is larger than that in the $h = 2$ case.

Using perturbation method, Chun and Baik (1994) investigated the weakly nonlinear response of a stably stratified uniform flow to diabatic forcing. The dynamical framework in their study is the same as that in the present study except that the prescribed heating is vertically homogeneous from the surface to a certain height. Their result indicated that the first-order solutions are valid for relatively small values of the nondimensional heating depth or the inverse Froude number because the solutions contain the $2z$ term. To examine in which way this kind of secular problem occurs for the exponentially decreasing heating profile with height, the domain maximum zeroth-order and first-order perturbation vertical velocities as a function of the e -folding heating depth are plotted in Figure 5. The heating depth is allowed to vary from $h = 0.5$ to 10 with a 0.5 increment. As the heating depth increases, the zeroth-order maximum vertical velocity gradually increases and then remains little changed. However, unlike the uniform heating case that shows increasing perturbation in an oscillatory behaviour with the increasing heating depth (Chun and Baik, 1994), the first-order maximum vertical velocity for the exponentially-decreasing vertical heating profile monotonously increases with the heating depth. Up to $h \sim 2.5$, the magnitudes of both the zeroth-order and first-order maximum vertical velocities are similar to each other.

From a dynamical point of view, it appears to be reasonable that precipitation is more likely to occur in the region of a low-level updraft than in the region of a low-level downdraft when other conditions are favourable. The linear solution part shows upward motion downstream (Figure 2), which partly explains precipitation enhancement observed on the downstream side of the heat island. On the other hand, the weakly nonlinear solution part shows downward or upward motion downstream depending on the heating depth, thus reducing or enhancing the zeroth-order upward motion induced by the stationary heating. Therefore, based on the present weakly nonlinear study, it is proposed that when the heating depth is large, but still within a valid range of the perturbation expansion, the linear and weakly nonlinear effects constructively work together to produce enhanced upward motion on the

downstream side, not far from the heating centre. This explains, to a greater extent than the linear effect alone, the precipitation enhancement downstream of the heat island. It is also proposed that when the heating depth is small, the linear and weakly nonlinear effects destructively work together to reduce upward motion on the downstream side, not far from the heating centre. This explains, to a lesser extent than the linear effect alone, the precipitation enhancement downstream of the heat island. If validity of the perturbation expansion is allowed up to $\max(w_1)/\max(w_0) \sim 2$, the weakly nonlinear solutions are valid up to $h \sim 4$ (see Figure 5).

The study has dealt with a steady-state, weakly nonlinear problem in a theoretical framework to explain some dynamical aspects of precipitation enhancement on the downstream side of an urban heat-island. When a time-dependency is included in a linear, theoretical framework, the air parcel ascends downwind of the heat island (Lin and Smith, 1986). When a time-dependency is included in a nonlinear numerical model framework, for smaller heating amplitude (hence, smaller nonlinearity factor) the flow response field is similar to that produced by the linear gravity waves, while for larger heating amplitude a strong updraft cell is observed downwind (Baik, 1992). This strong updraft cell can give an efficient impetus to moist convection or to the initiation of moist convection when other conditions are favourable. However, a steady-state, linear case produces the gravity-wave response field regardless of the heating amplitude.

4. Conclusions

Urban-rural circulations are similar to sea/land breezes and mountain/valley winds, in that it is the differential heating and cooling between the urban and rural areas that generate and sustain the wind system (Pielke, 1984). A lot of distinctive characteristics between the urban and rural areas such as the surface heat budget are combined to produce the urban heat island. Meteorological conditions also affect the intensity of the urban heat island (Oke, 1973). Mesoscale numerical models with advanced planetary boundary layer and surface parameterisations are very useful tools for examining physical processes involved in the urban heat-island phenomenon and related effects. Simple analytical models cannot treat fully nonlinear effects as can numerical models, but can provide a clear dynamical insight of some aspects of the phenomenon.

In this paper, we mainly investigated the effects of nonlinearity on the possible precipitation change downwind of the urban heat island by analytically solving the problem of the weakly nonlinear response of a stably stratified uniform flow to prescribed heating. It was shown that weakly nonlinearity effects, depending on the heating depth, can reduce or enhance an increase in precipitation downwind of the urban heat island, which is partly attributed to upward motion downwind in the linear studies. However, further study with a numerical model containing moist physics is needed to verify that the urban heat island-induced upward motion down-

wind is indeed capable of resulting in precipitation or an increase in precipitation on the downstream side of the urban heat island.

Acknowledgements

The first author was supported by the basic research fund of Kwangju Institute of Science and Technology and by the Korea Ministry of Science and Technology.

References

- Baik, J.-J.: 1992, 'Response of a Stably Stratified Atmosphere to Low-Level Heating – An Application to the Heat Island Problem', *J. Appl. Meteorol.* **31**, 291–303.
- Baik, J.-J. and Chun, H.-Y.: 1996, 'Effects of Nonlinearity on the Atmospheric Flow Response to Low-Level Heating in a Uniform Flow', *J. Atmos. Sci.* **53**, 1856–1869.
- Booker, J. R. and Bretherton, F. P.: 1967, 'The Critical Layer for Internal Gravity Waves in a Shear Flow', *J. Fluid Mech.* **27**, 513–539.
- Changnon, S. A., Shealy, B. T., and Scott, R. W.: 1991, 'Precipitation Changes in Fall, Winter, and Spring Caused by St. Louis', *J. Appl. Meteorol.* **30**, 126–134.
- Chun, H.-Y. and Baik, J.-J.: 1994, 'Weakly Nonlinear Response of a Stably Stratified Atmosphere to Diabatic Forcing in a Uniform Flow', *J. Atmos. Sci.* **51**, 3109–3121.
- Lin, Y.-L. and Chun, H.-Y.: 1991, 'Effects of Diabatic Cooling in a Shear Flow with a Critical Level', *J. Atmos. Sci.* **48**, 2476–2491.
- Lin, Y.-L. and Smith, R. B.: 1986, 'Transient Dynamics of Airflow near a Local Heat Source', *J. Atmos. Sci.* **43**, 40–49.
- Oke, T. R.: 1973, 'City Size and the Urban Heat Island', *Atmos. Environ.* **7**, 769–779.
- Olfe, D. B. and Lee, R. L.: 1971, 'Linearized Calculations of Urban Heat Island Convection Effects', *J. Atmos. Sci.* **28**, 1374–1388.
- Pielke, R. A.: 1984, *Mesoscale Meteorological Modeling*, Academic Press, 612 pp.
- Smith, R. B. and Lin, Y.-L.: 1982, 'The Addition of Heat to a Stratified Airstream with Application to the Dynamics of Orographic Rain', *Quart. J. Roy. Meteorol. Soc.* **108**, 353–378.